Phase-Coexistence and Thermal Hysteresis in Samples Comprising Adventitiously Doped MnAs Nanocrystals: Programming of Aggregate Properties in Magnetostructural Nanomaterials

Yanhua Zhang,[†] Rajesh Regmi,[‡] Yi Liu,[§,⊥] Gavin Lawes,[‡] and Stephanie L. Brock[†,*]

[†]Department of Chemistry, Wayne State University, Detroit, Michigan 48202, United States, [‡]Department of Physics and Astronomy, Wayne State University, Detroit, Michigan 48202, United States, and [§]Electron Microscopy Facility, Oregon State University, Corvallis, Oregon 77331, United States. [⊥]Present address: Technical Center, Chrysler LLC, 2301 Feather Stone Road, Auburn Hills, MI 48326.

ABSTRACT Small changes in the synthesis of MnAs nanoparticles lead to materials with distinct behavior. Samples prepared by slow heating to 523 K (type-A) exhibit the characteristic magnetostructural transition from the ferromagnetic hexagonal (α) to the paramagnetic orthorhombic (β) phase of bulk MnAs at Tp = 312 K, whereas those prepared by rapid nucleation at 603 K (type-B) adopt the β structure at room temperature and exhibit anomalous magnetic properties. The behavior of type-B nanoparticles is due to P-incorporation (up to 3%), attributed to reaction of the solvent (trioctylphosphine oxide). P-incorporation results in a decrease in the unit cell volume (~1%) and shifts Tp below room temperature. Temperature-dependent X-ray diffraction reveals a large region of phase-coexistence, up to 90 K, which may reflect small differences in Tp from particle-to-particle within the nearly monodisperse sample. The large coexistence range coupled to the thermal hysteresis results in process-dependent phase mixtures. As-prepared type-B samples exhibiting the β structure at room temperature convert to a mixture of α and β after the sample has been cooled to 77 K and rewarmed to room temperature. This change is reflected in the magnetic response, which shows an increased moment and a shift in the temperature hysteresis loop after cooling. The proportion of α present at room temperature can also be augmented by application of an external magnetic field. Both doped (type-B) and undoped (type-A) MnAs nanoparticles show significant thermal hysteresis narrowing relative to their bulk phases, suggesting that formation of nanoparticles may be an effective method to reduce thermal losses in magnetic refrigeration applications.

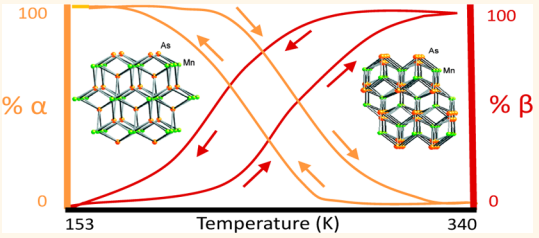

KEYWORDS: magnetic refrigeration · magnetocaloric effect · first-order phase transition · manganese arsenide · anion doping

"Smart" materials are those that exhibit a change in properties upon application of external stimuli, such as temperature, pressure, or an external magnetic or electric field. The biggest changes are observed at first-order phase transitions (FOPTs), which are identified by an abrupt (discontinuous) change of state and associated latent heat. Examples of FOPTs occurring between crystalline solids include the Martensic transition in shape-memory alloys,[1,2] the metal-to-insulator transition in VO_2[3] and the magnetostructural transition in MnAs and related alloys.[4] The ability to harness the release or absorption of latent heat enables exploitation in climate control devices. In the case of MnAs, there is a large magnetocaloric effect (MCE) associated with the magnetostructural transition, enabling heat release or absorption to be controlled by an external field, and making this material of interest for magnetic refrigeration.[5]

Traditional magnetic refrigeration materials are based on Gd, and therefore cost-prohibitive, resulting in an exploration of more earth-abundant and/or inexpensive materials.[6] In principle, bulk MnAs is a

* Address correspondence to sbrock@chem.wayne.edu.

Received for review February 26, 2014 and accepted June 3, 2014.

Published online June 03, 2014
10.1021/nn501149s

promising material for room temperature magnetic refrigeration applications due to the large magnetic entropy change, $\Delta S_M = -30$ J kg^{-1} K^{-1} (field change, $\Delta H = 5$ T), which is twice as large as $Gd_5Si_2Ge_2$ and three times larger than Gd.[7] The entropy change arises from the FOPT between the ferromagnetic hexagonal structure (NiAs-type, α) to the paramagnetic orthorhombic structure (MnP-type, β) at Tp = 308 (cooling)/315 (heating) K,[8] as shown in Figures S1 and S2 (Supporting Information). However, MnAs suffers from a large thermal hysteresis, 7 K, that precludes efficient cycling, yet the sharpness of the transition limits the temperature range for operation.[7] Substitution of Mn with Fe,[9,10] Cr,[11] Al,[12] or Si[13] can be used to tune the phase transition temperature and degree of hysteresis, providing a spectrum of materials to span a range suitable for climate control near room temperature. Anion doping is also effective for tuning MCE in MnAs; the FOPT is retained with up to 3% doping of P for As, shifting Tp from 315 down to 280 K (heating), but producing a temperature hysteresis of up to 30 K.[14] Recently, it has been shown that temperature hysteresis can be reduced in nanostructured materials prepared by ball-milling, with particle size and/or strain implicated as the governing factor.[15,16] However, the polydispersity of the samples and the inability to independently control size and strain preclude an assessment of how these factors influence the intrinsic properties of MnAs, including Tp and temperature hysteresis. Hence, we have established synthetic methods to prepare discrete particles of MnAs as monodisperse samples of controlled size in order to probe their size-dependent magnetic properties.[8,17]

Previously, we showed that when prepared on the nanoscale by arrested precipitation reactions at 523−603 K, MnAs nanoparticles corresponding to either α or β-structure can be isolated at room temperature (298 K).[17] Those samples that form the α-MnAs structure at room temperature (type-A MnAs nanoparticles) are prepared by slowly heating the Mn and As sources to 523 K in a solution of octadecene and trioctylphosphine oxide (TOPO). Type-A MnAs nanoparticles behave similarly to bulk MnAs and show the magnetostructural transition (Tp) near 312 K that is characteristic of MnAs, but with a decreased temperature hysteresis (<1 K, Figure S2, Supporting Information). In contrast, those samples that adopt the β-structure (type-B MnAs nanoparticles) at room temperature are prepared by rapid injection of $Mn_2(CO)_{10}$ in octadecene into a hot (603 K) solution of triphenylarsine oxide/TOPO. Type-B MnAs nanoparticles do not show a structural transition in the range 295 K − 335 K, as observed for bulk and type-A MnAs nanoparticles, but do exhibit ferromagnetism with a Curie temperature (T_C) near that of the Tp for bulk and type-A MnAs, calling into question the coupling between structure and magnetic exchange in this system.[8] A previous study showed that over several months at room temperature, the type-B MnAs nanoparticles partially converted from the β-phase to the thermodynamically stable α-phase, consistent with metastability in type-B MnAs nanoparticles.[12] However, the process is very slow and samples do not always convert, or convert completely.

To establish the origin of the apparent "kinetic trapping" of the β-structure in type-B MnAs nanoparticles, and the apparent decoupling of magnetic and structural phase transitions, we have undertaken a temperature-dependent powder X-ray diffraction study, performed nanoscale chemical analysis and structure analysis *via* STEM/EDS and HRTEM, and evaluated the role of magnetic and temperature history on the magnetic behavior and room-temperature structure of type-B MnAs nanoparticles. Here we demonstrate that type-B MnAs nanoparticles are distinguished from type-A by inadvertent P-doping, resulting in a compression of lattice parameters in MnAs, a concomitant decrease in the magnetostructural phase transition temperature, Tp, and the observation of a large temperature region of phase coexistence. We hypothesize that the solvent TOPO serves as the source of P dopant. The large coexistence range coupled to the thermal hysteresis results in process-dependent phase mixtures, making this material not just "smart" but also "programmable". The fact that MnAs nanoparticles are amenable to significant doping on the anionic lattice, even with poorly reactive dopant precursors, suggests a wide range of compositional space will be accessible for property tuning, thus enabling both size and dopant concentration to be independently tuned for optimization of properties relevant to magnetic refrigeration, sensing, and data storage.

RESULTS AND DISCUSSION

Structural and Compositional Analyses. Approximately 20 nm type-A and type-B MnAs nanocrystals were synthesized following our reported procedure with some modifications.[12] Briefly, type-A is prepared by combining $Mn_2(CO)_{10}$ and triphenylarsine oxide in a mixture of 1-octadecene and trioctylphosphine oxide (TOPO) and gradually heating to 523 K under inert atmosphere (slow heating method), whereas type-B is prepared by cannulating $Mn_2(CO)_{10}$ dissolved in octadecene into a mixture of triphenylarsine oxide in TOPO at 603 K (rapid injection method). Room temperature XRD and TEM characterization data for type-A and type-B MnAs nanoparticles can be found in the Supporting Information (Figures S3−S5). Both MnAs nanoparticle samples presented in this work are narrowly polydisperse: type-A = 22.3 ± 3.9 and type-B = 21.1 ± 1.2 nm in diameter.

On the basis of the observation that type-B nanoparticles occasionally convert from β to α at room

TABLE 1. Lattice Parameter and Cell Volume Data for Bulk and Nanoparticulate (Types A and B) MnAs[a]

material	*a* (Å)	*b* (Å)	*c* (Å)	cell volume (Å^3)
Bulk	5.734(3)	3.684(3)	6.378(4)	134.729(1)
Type-A Nano	5.728(4)	3.686(5)	6.379(9)	134.682(2)
Type-B Nano	5.713(3)	3.672(5)	6.356(9)	133.337(2)

[a] Comparison at 335 K, orthorhombic β-model. Lattice parameters reproduced from ref 8.

temperature (whereas type-A nanoparticles only exist as α at room temperature), we initially hypothesized that the type-B nanoparticles may be trapped in a metastable state having the β-structure, perhaps due to strain attributed to the high temperature and rapid nucleation inherent in the synthesis. Accordingly, we sought to promote the transformation from β to α in type-B nanoparticles by heating the sample to overcome the kinetic barrier. However, treatment at temperatures up to 393 K did not result in any change in the phase observed by XRD at room-temperature (β, Figure S6, Supporting Information). This suggests that the transformation of β to α in type-B MnAs nanocrystals cannot be explained by a conventional thermal energy barrier.

A careful evaluation of Pair Distribution Function Analysis data previously acquired on type-B MnAs nanoparticles reveals a significant isotropic compression of unit cell parameters relative to bulk MnAs and type-A MnAs nanoparticles at 335 K (above Tp, β structure fit, Table 1).[8] Type-A MnAs demonstrates only a small contraction in unit cell volume (0.035(2)%) relative to bulk MnAs, whereas the unit cell volume for type-B MnAs nanoparticles is decreased by 1.033(2)%. Because of the magneto-structural coupling, such small changes in lattice parameters are known to have a dramatic effect on the relative energies of the two phases (ferromagnetic *vs* paramagnetic) in the bulk, resulting in a change in Tp.[4,18] Accordingly, we hypothesized that Tp for type-B MnAs nanoparticles may occur at a lower temperature due to significant lattice parameter compression arising from surface strain,[19] or atomic substitution on the anionic or cationic lattice with an impurity ion of smaller radius.[14,20]

To evaluate whether type-B MnAs nanoparticles are inadvertently doped, the elemental composition of individual nanoparticles was analyzed using high angle annular dark field scanning transmission electron microscopy (HAADF-STEM) combined with elemental analysis (EDS). Figure 1 shows a HAADF-STEM image and elemental mapping (EDS) for type-B MnAs. The particles consist of a high-contrast core and a low-contrast shell. For Mn and As, the signal is very intense in both the crystalline core and the amorphous shell of the nanoparticles, and these two components rise and fall together (Figure 1). This is consistent with a

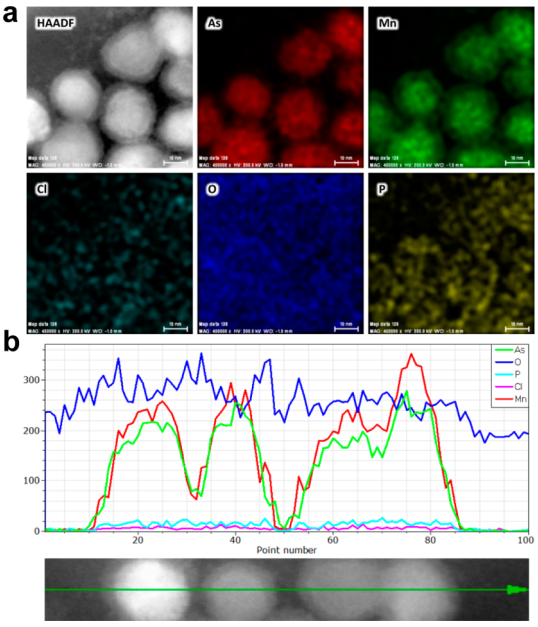

Figure 1. (a) HAADF-STEM of type-B MnAs nanoparticles and EDS elemental analysis maps for Mn, As, O, P and Cl, respectively. The scale bar corresponds to 10 nm. (b) Line profile elemental analysis for several single Type-B MnAs nanoparticles (image at bottom) showing that Mn (red) and As (green) rise and fall together and that there is a discernible quantity of P (turquoise) that tracks Mn and As. Cl (pink) and O (blue) are also found as background signals and attributed to the solvent $CHCl_3$ and ethanol/air oxidation, respectively.

previous IR study that revealed the presence of Mn arsenate (or −ite), presumably arising from inadvertent oxidation of MnAs,[17] (although we cannot rule out the simultaneous presence of a carbonaceous coating, as is observed in FeAs nanoparticles prepared under similar conditions[21]). However, there is also a trace amount of P in the shell and in the core, and this is seen consistently upon analysis of two independent samples of type-B nanoparticles. The most likely source of P in our reaction is the decomposition of the coordinating solvent, TOPO. While TOPO has historically been considered to be an inert solvent for nanocrystal formation, recent work has shown that use of TOPO results in adventitious doping of P in Co nanoparticles,[22] and TOPO can be used as the P-source in Co_2P nanoparticle formation at temperatures as low as 603 K, the synthesis temperature for Type-B MnAs nanoparticles.[23] Inductively Coupled Plasma-Optical Emission Spectroscopy (ICP-OES) analysis of Mn and P in the type-B nanoparticle sample (Table S1, Supporting Information) is consistent with the HAADF-STEM/EDS data, suggesting a formulation of $MnAs_{0.972}P_{0.028}$ (based on the Mn:P ratio and assuming an overall 1:1 Mn:Pn, Pn = As, P ratio). In contrast, HAADF-STEM/EDS analyses of similarly sized type-A MnAs nanoparticles (Figure S7, Supporting Information) do not show any signal for P or evidence of any other dopant in the particles. Likewise, the phosphorus concentration in Type A

nanoparticles was below the detection limit of ICP-OES (Table S1, Supporting Information).

On the basis of the compositional data, the atomic substitution of P for As is likely responsible for the decreased unit cell volume of type-B MnAs nanoparticles relative to bulk MnAs phase, although the magnitude of the change is smaller for the nanoparticles (1.0%) than for bulk (1.8%),[14] assuming 3% P inclusion. This may reflect a lower degree of P incorporation into the lattice of nanocrystalline MnAs than suggested by chemical analysis, perhaps due to partitioning to the amorphous arsenate (ite) shell. The structural properties and stability regions for α-type and β-type $MnAs_{1-x}P_x$ in the bulk phase depend sensitively on x, with Tp (measured upon heating) decreasing from ~315 to ~280 K as x increases from 0 to 0.03.[14] The extent of temperature hysteresis is also dependent upon the degree of doping; thus Tp recorded upon cooling ranges from ~305 (x = 0) to ~250 K (x = 0.03) corresponding to an increase in the temperature hysteresis from ΔT = 10 K (x = 0) to 30 K (x = 0.03).[14,20] For x > 0.03, the low temperature α phase is no longer stable at ambient pressure (*i.e.*, the material is β-phase for all T below the high temperature second order phase transition from paramagnetic β-$MnAs_{1-x}P_x$ to paramagnetic α-$MnAs_{1-x}P_x$, ~400−500 K, Figure S1, Supporting Information).[20] Thus, a consequence of unit cell compression due to P-doping in nanoscale MnAs is expected to be a decrease in Tp relative to that of pure MnAs nanoparticles (Tp = 315 K), resulting in room-temperature stability of the β-MnAs structure.[20]

To test the premise that Tp is decreased in type-B MnAs particles relative to type-A, T-dependent XRD studies were undertaken for type-B MnAs particles in the range 123−323 K. Figure 2a shows a series of XRD scans of the as-prepared type-B MnAs nanoparticles acquired upon cooling from 298−123 K, and then upon reheating to 323 K. Scans were taken at 25−30 K intervals in the 2θ region 47−53°, where the (110) reflection of α-MnAs and the (013) reflection of β-MnAs are easily distinguished. Upon cooling from 298 K past 273 K, the (013) peak of β-MnAs first shifts to higher 2θ, indicative of a large unit cell compression that reflects the strong thermal dependence of the lattice parameters in this structure. By 243 K, the (110) peak of α-MnAs is apparent, and conversion of β to α is complete by 153 K. However, warming back to 298 K (room temperature) does not result in complete conversion of α back to β. While the beginning of the conversion is apparent by 213 K, it is not complete until 323 K. This suggests that the transformation of type-B MnAs nanoparticles from β to α on cooling is reversible upon warming, but occurs with significant hysteresis and an extensive region of phase coexistence (as much as 90 K). Accordingly, the relative quantities of α- and β-MnAs depend on the temperature and the process history (cooling or warming) of the sample.

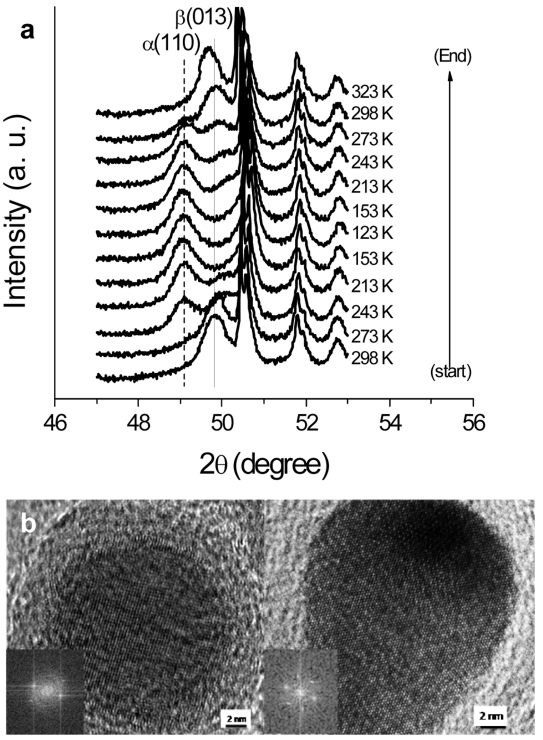

Figure 2. (a) Temperature dependent XRD for type-B MnAs nanoparticles upon cooling from 298 to 123 K and then warming back to 323 K (from bottom to top); nonindexed peaks arise from the Ni−Cu alloy sample holder. (b) Room temperature high resolution TEM images and FFT processing of an as-prepared type-B MnAs nanocrystal (left) and a type-B MnAs nanocrystal subjected to a cooling step at 77 K (right). Cooling (performed *ex situ*) has transformed the sample to the α-MnAs structure type. Differences in the particle shape and shell contrast can be attributed in part to variation from particle to particle. The shell of the particle at right is more evident in a larger field-of-view, as shown in Figure S8, Supporting Information.

The presence of a large coexistence range in type-B MnAs nanocrystals is in contrast to bulk materials, where coexistence is not reported, in keeping with the Gibbs phase rule that states that phases of the same chemical composition can only coexist at a single temperature.[24] However, previous studies on relatively large (*ca.* 80 nm diameter) MnAs disks grown epitaxially on GaAs(001) showed that over the entire sample, a large (45 K) range of coexistence is present; however, each disk remains single domain, and undergoes an instantaneous transformation that is predicated upon the formation of a stable nuclei of the other phase within the disk (estimated to be growth to 18 nm in diameter).[25] Given the small size of our MnAs nanocrystals (*ca.* 20 nm), it is likely that transformations within individual particles are occurring abruptly, and the coexistence range is due to heterogeneity in the sample. Such heterogeneity may arise from differential P-doping levels or other defects among particles, as well as small variations in size, shape and surface characteristics.

Figure 2b shows evidence for the complete transformation of individual MnAs nanocrystals. High-resolution

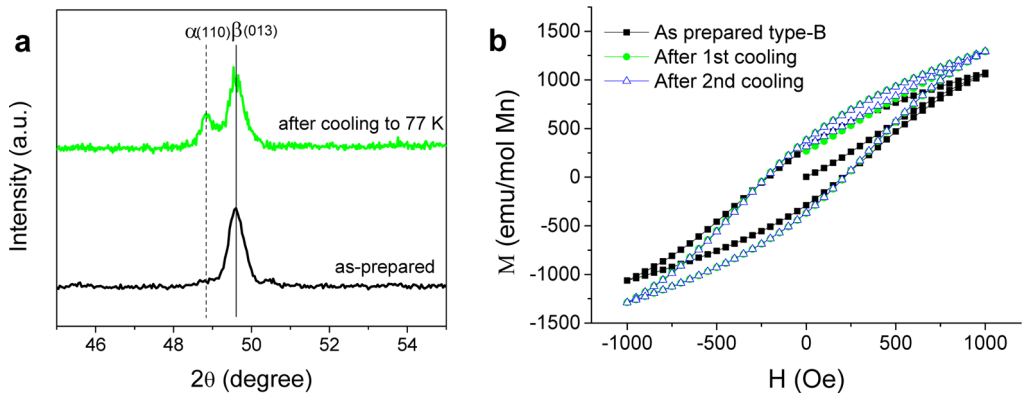

Figure 3. (a) Room temperature XRD and (b) 300 K DC magnetization acquired before and after cooling as-prepared type-B MnAs nanoparticles to 77 K.

transmission electron microscopy (HRTEM) images of representative type-B MnAs nanocrystals (acquired at room temperature) before and after cooling to 77 K show the uniformity of the lattice throughout the nanocrystal. Fast Fourier Transform (FFT) processing of the images reveals that the as-prepared particles adopt the orthorhombic β structure, whereas the previously cooled samples exhibit the hexagonal α structure.

A consequence of the coexistence range extending to room temperature is that bulk characterization conducted at ambient temperatures may reflect differing quantities of each phase depending on how the sample was treated. Thus, XRD data on as-prepared samples, cooled to room temperature from the high-temperature conditions employed in the synthesis (603 K), typically show β-MnAs. However, samples cooled to liquid nitrogen temperature (77 K) and then allowed to warm to room temperature show a mixture of phases, as shown in Figure 3a.

Consequences of the Phase Transition on Magnetic Properties. Because the structure and the magnetic properties are highly correlated in MnAs, we expect the structural behavior will be mirrored in the magnetic behavior. Bulk $MnAs_{1-x}P_x$ ($0 \leq x \leq 0.03$) is paramagnetic above Tp when it adopts the β structure, and is ferromagnetic when cooled below Tp as the structure converts from low to high spin and transforms to α. Thus, the Curie Temperature, Tc, of the magnetic phase should correspond to Tp.

Molar magnetization data on 21 nm type-B MnAs nanocrystals adopting the β structure are shown in Figure 4. The temperature range studied was limited in an attempt to remain in the coexistence range for α and β (*i.e.*, to avoid complete conversion to α, see ref 17). Data were acquired first on cooling, and then on heating, to ensure that the cooling curve corresponds most closely to the native behavior of as-prepared type-B MnAs nanoparticles (exclusively β-phase by XRD). It is evident that the type-B MnAs nanocrystals undergo a ferromagnetic transition upon cooling

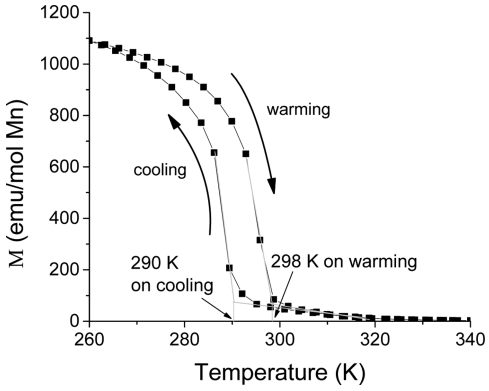

Figure 4. Temperature dependent dc molar magnetization data of type-B MnAs nanoparticles acquired at 100 Oe. The cooling profile (from 340 K) was acquired first in order to capture the native properties of as-prepared Type-B MnAs.

below 290 K and that there is a significant hysteresis upon warming due to the thermal losses during the magnetostructural transition, so that the transition is closer to 300 K. These data are somewhat shifted relative to the temperature-dependent XRD data where the first evidence of α-phase formation occurred upon cooling below 273 and significant α remains upon reheating to room temperature (298 K). This likely reflects the responsiveness of molar magnetization measurements to even small weight fractions of ferromagnetic components within an otherwise paramagnetic system. In keeping with the observation of a region of phase coexistence extending (conservatively) down to 213 K (Figure 2a) upon cooling, the magnetization has not saturated at the lowest measured temperature (260 K). In contrast, type-A MnAs nanoparticles exhibit a higher transition temperature (~312 K) and the magnetization is saturated by 300 K, more closely mapping to bulk MnAs (Figure S2, Supporting Information).[8]

In contrast to type-B, type-A MnAs nanoparticles demonstrate minimal temperature hysteresis (Figure S2, Supporting Information); type-A samples exhibit hysteresis of <1 K relative to 7 K for type B. Such an

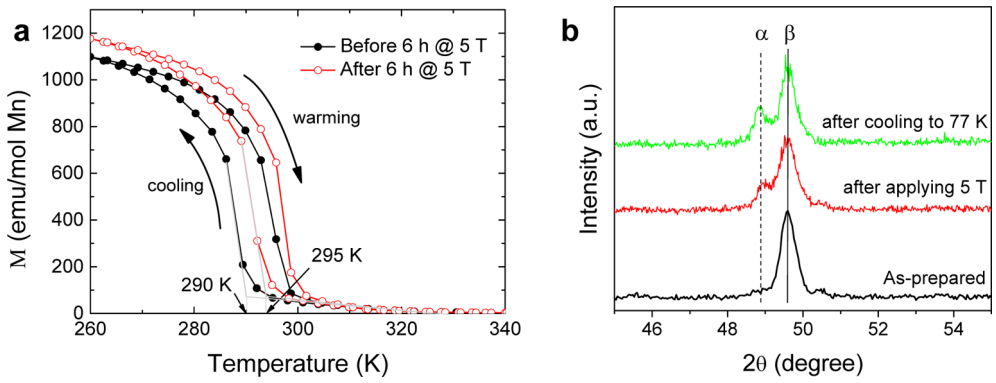

Figure 5. (a) AC magnetization (collected at 100 Oe) of type-B MnAs nanocrystals before and after applying a 5 T field; (b) room temperature XRD data comparing the effect of having cooled type-B MnAs nanoparticles with having treated them with a 5 T field.

increase is expected upon doping, but is actually far smaller than that reported for bulk $MnAs_{0.97}P_{0.03}$ (30 K). Reduction of thermal hysteresis (from 10−30 to 2−4 K) has been demonstrated in $MnAs_{1-x}P_x$ (x = 0.006 and 0.01) prepared by ball milling (polydisperse samples, with sizes ranging from 200 nm-4 μm in diameter).[15] However, it is not clear whether the decreased hysteresis is due to size or strain effects, since a similar study for x = 0.03 reported significant strain in as-prepared ball-milled nanoparticles with crystallite sizes of 23 nm (from application of the Scherrer eq to XRD data). Release of strain occurs upon annealing, and is accompanied by an increase in hysteresis from 2 to 10 K, but this is also accompanied by crystallite growth to over 100 nm.[16] It is worth noting that in addition to the significant decrease in temperature hysteresis we see for 21 nm $MnAs_{0.97}P_{0.03}$ nanocrystals relative to bulk (microcrystalline) samples, type-A MnAs nanoparticles also exhibit minimal temperature hysteresis when compared to bulk MnAs (7 K, Figure S2, Supporting Information),[8] lending credence to the notion that minimizing particle size can have a large effect on thermal losses in these materials, an important criterion for applications in magnetic refrigeration.

Intriguingly, magnetization *vs* field data acquired at room temperature suggest the presence of some α-MnAs phase in as-prepared type-B MnAs. As shown in Figure 3b, there is significant field hysteresis in as-prepared type-B nanoparticles, suggesting the presence of a ferromagnetic component (α-MnAs) that is not apparent in XRD (Figure 3a). On the basis of our prior work investigating MnP inclusions in chalcopyrites, the α-MnAs may amount to as much as 5 wt % of the sample.[26] An increase in the magnetization is apparent after cooling the sample to 77 K, and correlates with the observation of a discernible α peak in the room temperature XRD, indicative of a shift in the population of α and β at room temperature due to the low temperature processing.

As for bulk MnAs,[27] the population shift in type-B MnAs nanoparticles can also be induced by changes in applied magnetic field; a 5 h isothermal treatment of as-prepared type-B MnAs nanoparticles results in a distinct increase in the net magnetization and a shift in the Tc onset (cooling) from 291 to 297 K, suggesting some transformation has occurred (Figure 5a). The corresponding XRD data for samples either cooled or to which a 5 T field was applied are presented in Figure 5b and show that the transformations induced by cooling or by applying an external field are comparable. As with the T-dependent XRD data (Figure 2a), we surmise this history-dependent phase stability arises from applying perturbations to the sample within the phase coexistence temperature region. The temperature history dependence of Tc now explains our original (erroneous) claim that type-A and type-B nanoparticles had the same Tc;[17] those data were all acquired upon heating from 10K, and can therefore be expected to shift the temperature loop to higher temperatures, approaching that of pure MnAs.

CONCLUSIONS

MnAs nanoparticles prepared in solution by rapid injection unintentionally incorporate small amounts of P (~3%) when trioctylphosphine oxide is used as a solvent. The structural consequences of doping are a decrease in the first order phase transformation temperature from the hexagonal (α) to the orthorhombic (β) structure, also characteristic of the bulk doped phase, and an extensive temperature range of phase-coexistence within the bulk sample (although transformation within individual nanoparticles appears to be abrupt), which is unique to the nanoscale formulation. Thus, the proportion of α and β observed at room temperature depends sensitively on the temperature processing of the sample, and can also be tuned by magnetic field, making the behavior effectively "programmable". At the same time, the decreased particle size results in decreased thermal hysteresis for the magnetic transition relative to bulk samples for both doped and undoped samples, suggesting that reduction in particle size may be an effective method to

reduce thermal losses associated with the transition. The ability to reduce such thermal losses during cycling and to tune transition temperature over a moderate range suggests such materials may be suitable for room temperature magnetic refrigeration applications. Current work is focused on elucidating the mechanism of P-doping, controlling doping by use of a more reactive source (*e.g.*, trioctylphosphine) and assessing the magnetic entropy associated with the phase transformation in MnAs and doped nanoparticles.

METHODS

Materials. Manganese carbonyl (98%), triphenylarsine oxide (97%), 1-octadecene (90%, tech grade), and trioctylphosphine oxide (TOPO, 90%, tech grade) were purchased from Sigma-Aldrich, Inc. TOPO was purified by distillation and recrystallization as described by Buhro and co-workers.[28] All other chemicals were used as received.

Synthesis. Type-B MnAs nanocrystals were synthesized following the previous reported method[8] with slight modifications. A total of 0.5 mmol of $Mn_2(CO)_{10}$, and 10 mL of 1-octadecene are mixed together in the glovebox, then placed in a Schlenk flask followed by argon flushing and evacuation cycles over a period of 15 min. Before injection, the mixture is slightly warmed with a heat gun until the powder precursors are dissolved. The mixture is then cannulated under inert conditions (Ar) into a 603 K solution consisting of 5 g of TOPO and 1 mmol of triphenylarsine oxide. The reaction was maintained at 603 K for 5 h. The final product was dispersed in chloroform and precipitated with ethanol several times and then dried under vacuum.

Type-A MnAs nanoparticles were synthesized by combining the reagent amounts indicated above in a single Schlenk flask. After Ar flushing and evacuation (described above), the solution was gradually heated to 523 at 1 K/min. The product was isolated as described above.

Characterization. Room temperature powder X-ray diffraction (XRD) data were acquired on a Rigaku 200 B model X-ray diffractometer equipped with a rotating Cu anode source. Samples were placed on a zero-background quartz plate for measurement. To assess whether heating would alter the proportion of α and β, as-prepared samples on the quartz sample plate were heated in an oven for 30 min at 400 K, allowed to return to room temperature, and then re-evaluated by XRD.

T-dependent XRD data in the 2θ range 47−53° were collected on a PANalytical X'Pert Pro diffractometer with temperature variation using the Scintag XDS-2000 accessory equipped with a Moxtek detector and an Anton Parr stage. MnAs powder was gently loaded on the thermal conductive alloy holder. Liquid nitrogen was used to cool the sample and a platinum heat strip was used to heat the sample. The sample was kept for 15 min at each measuring temperature to equilibrate. The 2θ scanning speed was 1°/min from 47° to 53°. The total temperature dependent study was performed in the temperature range 123−323 K with the heating/cooling rate 1 K/min.

Transmission electron microscopy (TEM) images and HRTEM images were acquired using a JEOL 2010 HR transmission electron microscope operated at 200 kV. The samples were prepared by placing one drop of chloroform containing the dispersion of MnAs nanoparticles onto a 200 mesh Cu grid coated with a carbon film.

Scanning Transmission Electron Microscopy (STEM) data were taken using a FEI Titan 80-200 Field Emission Scanning Transmission Electron Microscope (S/TEM) operated at 200 kV. In STEM mode, Z-contrast images were taken using a high-angle annular dark-field (HAADF) detector (Fischione Instruments), and elemental mapping was performed using the "X" Energy Dispersive Spectrometric (EDS) system consisting of 4 windowless silicon-drift detectors (SDD) positioned symmetrically around the specimen in a unique FEI design. The SSDs are made by PN Sensors utilizing a pulse processor from Bruker. The integration of Super X EDS detection in combination with the High-Brightness Electron source is called ChemiSTEM Technology and was introduced by FEI in 2010. Samples were prepared as described in the section on transmission electron microscopy.

Elemental Analysis data (P:Mn ratio) were acquired on a Horiba Ultima Inductively Coupled Plasma-Optical Emission Spectroscopy (ICP-OES) instrument. MnAs nanoparticles (~2 mg) were dissolved in 1.5 mL concentrated nitric acid and then diluted to 50 mL using a 50 mL volumetric flask. 2% HNO_3 solution was used as blank. Mn standard solutions (1, 5, 10, and 20 ppm) and P standard solutions (10 ppb, 50 ppb, 0.2 ppm and 0.5 ppm) were used to calibrate the instrument.

Molar Magnetization Measurements were acquired on solid samples of MnAs nanoparticles sealed under vacuum in fused silica tubes. DC data were acquired on a Quantum Design MPMS 5S and AC data on a Quantum Design PPMS 6000. Temperature-dependent molar magnetization data were acquired in an applied field of 100 Oe upon cooling from 340 to 260 K, and then upon heating back to 340 K. Data were also acquired after application of a 5 T field for 6 h at 300 K. Molar magnetization *vs* field data were acquired at 300 K upon sweeping from −1000 to 1000 Oe. All data were normalized to moles of Mn in the sample, determined by Atomic Absorption performed on a Perkin-Elmer AAnalyst 700 Atomic Absorption Spectrometer with flame. Samples were dissolved in nitric acid as described for ICP and referenced to Mn calibration standards.

Conflict of Interest: The authors declare no competing financial interest.

Acknowledgment. Y.Z. and S.L.B. acknowledge NSF DMR 1064159. R.R. and G.L. acknowledge NSF DMR 0644823 and 1306449. HAADF/STEM data were acquired on a FEI Titan 80-200 field emission transmission electron microscope with ChemiSTEM technology purchased with funds provided by NSF MRI award 1040588, the Murdock Charitable Trust and Oregon Nanoscience and Microtechnologies Institute (ONAMI). TEM and HRTEM data were acquired on a JEOL 2010 TEM with funds provided by NSF MRI award 0216084. TEM, ICP, AA and routine powder X-ray diffraction were acquired at the Lumigen Instrument Center, Wayne State University. Temperature-dependent powder X-ray diffraction measurements were acquired at the Instrumentation Center, University of Tolelo. We thank Jan Musfeldt for helpful conversations, Pannee Burkel for assistance with temperature-dependent X-ray, and Ambesh Dixit for assistance with magnetic data collection and interpretation.

Supporting Information Available: ICP-data (table); scheme of the magnetostructural transformation, molar magnetization data for MnAs (bulk) and type-A MnAs nanoparticles, XRD data for type-A and type-B MnAs nanoparticles, TEM data and histogram for type-B MnAs nanoparticles, XRD data showing the effect of heating on type-B MnAs nanoparticles, HAADF-STEM EDS mapping of type-A MnAs nanoparticles, expanded TEM micrograph of Type-B nanoparticles after cooling (figures). This material is available free of charge *via* the Internet at http://pubs.acs.org.

REFERENCES AND NOTES

1. Cui, J. Shape Memory Alloys and Their Applications in Power Generation and Refrigeration. *Mater. Res. Soc. Symp. Proc.* **2013**, *1581*, 737–1-12.
2. Omori, T.; Kainuma, R. Materials Science: Alloys with Long Memories. *Nature* **2013**, *502*, 42–44.
3. Whittaker, L.; Patridge, C. J.; Banerjee, S. Microscopic and Nanoscale Perspective of the Metal−Insulator Phase

Transitions of VO_2: Some New Twists to an Old Tale. *J. Phys. Chem. Lett.* **2011**, *2*, 745–758.
4. Goodenough, J. B.; Kafalas, J. A. High-Pressure Study of the First-Order Phase Transition in MnAs. *Phys. Rev.* **1967**, *157*, 389–395.
5. Franco, V.; Blázquez, J. S.; Ingale, B.; Conde, A. The Magnetocaloric Effect and Magnetic Refrigeration Near Room Temperature: Materials and Models. *Annu. Rev. Mater. Res.* **2012**, *42*, 305–342.
6. Tan, X.; Chai, P.; Thompson, C. M.; Shatruk, M. Magnetocaloric Effect in $AlFe_2B_2$: Toward Magnetic Refrigerants from Earth-Abundant Elements. *J. Am. Chem. Soc.* **2013**, *135*, 9553–9557.
7. Wada, H.; Tanabe, Y. Giant Magnetocaloric Effect of $MnAs_{1-x}Sb_x$. *Appl. Phys. Lett.* **2001**, *79*, 3302–3304.
8. Tian, P.; Zhang, Y.; Senevirathne, K.; Brock, S. L.; Dixit, A.; Lawes, G.; Billinge, S. J. L. Diverse Structural and Magnetic Properties of Differently Prepared MnAs Nanoparticles. *ACS Nano* **2011**, *5*, 2970–2978.
9. Balli, M.; Fruchart, D.; Gignoux, D.; Zach, R. The "Colossal" Magnetocaloric Effect in $Mn_{1-x}Fe_xAs$: What Are We Really Measuring? *Appl. Phys. Lett.* **2009**, *95*, 072509-1–3.
10. Bratko, M.; Morrison, K.; de Campos, A.; Gama, S.; Cohen, L. F.; Sandeman, K. G. History Dependence of Directly Observed Magnetocaloric Effects in (Mn,Fe)As. *Appl. Phys. Lett.* **2012**, *100*, 252409–1-4.
11. Sun, N. K.; Cui, W. B.; Li, D.; Geng, D. Y.; Yang, F.; Zhang, Z. D. Giant Room-Temperature Magnetocaloric Effect in $Mn_{1-x}Cr_xAs$. *Appl. Phys. Lett.* **2008**, *92*, 072504-1–3.
12. Cui, W. B.; Liu, W.; Liu, X. H.; Guo, S.; Han, Z.; Zhao, X. G.; Zhang, Z. D. Beneficial Effect of Minor Al Substitution on the Magnetocaloric Effect of $Mn_{1-x}Al_xAs$. *Mater. Lett.* **2009**, *63*, 595–597.
13. Cui, W. B.; Liu, W.; Liu, X. H.; Guo, S.; Han, Z. Magnetocaloric Effects and Reduced Thermal Hysteresis in Si-Doped MnAs Compounds. *J. Alloys Compd.* **2009**, *479*, 189.
14. Roger, A.; Fruchart, R. Etude Magnetique et Structural de la Solution Solide MnP-MnAs. *Mater. Res. Bull.* **1968**, *3*, 253–264.
15. Sun, N.; Xu, S.; Li, D.; Zhang, Z. Magnetocaloric Effect and Size-effect Related Thermal Hysteresis Reduction in $MnAs_{1-x}P_x$ Compounds. *Phys. Status Solidi A* **2011**, *208*, 1950–1952.
16. Sun, N. K.; Liu, F.; Gao, Y. B.; Cai, Z. Q.; Du, B. S.; Xu, S. N.; Si, P. Z. Effect of Microstrain on the Magnetism and Magnetocaloric Properties of $MnAs_{0.97}P_{0.03}$. *Appl. Phys. Lett.* **2012**, *100*, 112407–1-4.
17. Senevirathne, K.; Tackett, R.; Kharel, P.; Lawes, G.; Somaskandan, K.; Brock, S. L. Discrete, Dispersible MnAs Nanocrystals from Solution Methods: Phase Control on the Nanoscale and Magnetic Consequences. *ACS Nano* **2009**, *3*, 1129–1138.
18. Iikawa, F.; Brasil, M. J. S. P.; Adriano, C.; Couto, O. D. D.; Giles, C.; Santos, P. V.; Däweritz, L.; Rungger, I.; Sanvito, S. Lattice Distortion Effects on the Magnetostructural Phase Transition of MnAs. *Phys. Rev. Lett.* **2005**, *95*, 077203–1-4.
19. Takagaki, Y.; Jenichen, B.; Herrmann, C.; Wiebicke, E.; Däweritz, L.; Ploog, K. H. First-Order Phase Transition in MnAs Disks on GaAs (001). *Phys. Rev. B* **2006**, *73*, 125324-1–5.
20. Fjellvag, H.; Andresen, A. F.; Bärner, K. On the Magnetic and Structural Properties of the $MnAs_{1-x}P_x$ System ($x \leqslant 0.18$). *J. Magn. Magn. Mater.* **1984**, *46*, 29–39.
21. Desai, P.; Song, K.; Koza, J.; Pariti, A.; Nath, M. Soft-Chemical Synthetic Route to Superparamagnetic FeAs@C Core–Shell Nanoparticles Exhibiting High Blocking Temperature. *Chem. Mater.* **2013**, *25*, 1510–1518.
22. Iablokov, V.; Beaumont, S. K.; Alayoglu, S.; Pushkarev, V. V.; Specht, C.; Gao, J.; Alivisatos, A. P.; Kruse, N.; Somorjai, G. A. Size-Controlled Model Co Nanoparticle Catalysts for CO_2 Hydrogenation: Synthesis, Characterization, and Catalytic Reactions. *Nano Lett.* **2012**, *12*, 3091–3096.
23. Zhang, H.; Ha, D.-H.; Hovden, R.; Kourkoutis, L. F.; Robinson, R. D. Controlled Synthesis of Uniform Cobalt Phosphide Hyperbranched Nanocrystals Using Tri-*n*-octylphosphine Oxide as a Phosphorus Source. *Nano Lett.* **2010**, *11*, 188–197.
24. Kaganer, V. M.; Jenichen, B.; Schippan, F.; Braun, W.; Däweritz, L.; Ploog, K. H. Strain-Mediated Phase Coexistence in Heteroepitaxial Films. *Phys. Rev. Lett.* **2000**, *85*, 341–344.
25. Jenichen, B.; Takagaki, Y.; Ploog, K. H.; Darowski, N.; Feyerherm, R.; Zizak, I. Nucleation at the Phase Transition Near 40 °C in MnAs Nanodisks. *Appl. Phys. Lett.* **2006**, *89*, 051915–1-3.
26. Aitken, J. A.; Tsoi, G.; Wenger, L. E.; Brock, S. L. Phase Segregation of MnP in Chalcopyrite Dilute Magnetic Semiconductors: A Cautionary Tale. *Chem. Mater.* **2007**, *19*, 5272–5278.
27. Mira, J.; Rivadulla, F.; Rivas, J.; Fondado, A.; Guidi, T.; Caciuffo, R.; Carsughi, F.; Radaelli, P. G.; Goodenough, J. B. Structural Transformation Induced by Magnetic Field and "Colossal-like" Magnetoresistance Response above 313 K in MnAs. *Phys. Rev. Lett.* **2003**, *90*, 097203-1–4.
28. Wang, F.; Tang, R.; Kao, J. L. F.; Dingman, S. D.; Buhro, W. E. Spectroscopic Identification of Tri-*n*-octylphosphine Oxide (TOPO) Impurities and Elucidation of Their Roles in Cadmium Selenide Quantum-Wire Growth. *J. Am. Chem. Soc.* **2009**, *131*, 4983–4994.